Journal of Catalysis **210,** 207–217 (2002)
doi:10.1006/jcat.2002.3681

Effect of Phosphorus Content in Nickel Phosphide Catalysts Studied by XAFS and Other Techniques

S. T. Oyama,*,[1] X. Wang,* Y.-K. Lee,* K. Bando,† and F. G. Requejo‡

*Environmental Catalysis and Materials Laboratory, Department of Chemical Engineering (0211), Virginia Polytechnic Institute and State University, Blacksburg, Virginia 24061; †National Institute of Advanced Industrial Science and Technology, AIST Tsukuba Central 5, 1-1-1, Higashi, Tsukuba, Ibaraki 305-8565, Japan; and ‡Departamento de Física, Faculdad de Ciencias Exactas, Universidad Nacional de la Plata and IFLP, CONICET, CC/67-1900 La Plata, Argentina

Received February 14, 2002; revised May 6, 2002; accepted May 20, 2002

A series of novel, high-activity supported nickel phosphide hydroprocessing catalysts (Ni_2P/SiO_2) was synthesized by means of temperature-programmed reduction (TPR), and the effect of phosphorus content on hydroprocessing performance and catalyst structure was studied. The catalysts were characterized by BET surface area determinations, CO uptake titrations, X-ray diffraction (XRD) analysis, elemental analysis, and extended X-ray absorption fine structure (EXAFS) measurements. The activity of the catalysts was studied in a three-phase trickle-bed reactor operated at 3.1 MPa and 643 K in the hydrodenitrogenation (HDN) and hydrodesulfurization (HDS) of a model liquid feed containing 2000 ppm nitrogen (quinoline), 3000 ppm sulfur (dibenzothiophene), 500 ppm oxygen (benzofuran), 20 wt% aromatics (tetralin), and balance aliphatics (tetradecane). The samples were prepared with initial Ni/P ratios of 2/1, 1/1, 1/1.8, 1/2, 1/2.2, and 1/3, but the samples with excess P lost some of their P content during reduction and the main phase obtained was Ni_2P. Activity and stability of the catalysts were affected profoundly by the phosphorus content, both reaching a maximum with an initial Ni/P ratio of about 1/2 (actual Ni/P = 1/0.57 after reaction). At this optimal P content, the activity was excellent, with steady state HDS conversion of 100% and HDN conversion of 81%, which were much higher than that of a commercial Ni–Mo–S/Al_2O_3 catalyst with corresponding HDN conversion of 76% and HDN conversion of 38%. The stability of the optimal composition was also high, with no deactivation observed over 90 h in HDS and only a slight deactivation in HDN. EXAFS analysis of the catalysts indicated the formation of a Ni_2P phase for the sample with an initial Ni/P ratio of 1/2, which was retained after reaction. At lower P content some Ni metal and $Ni_{12}P_5$ was obtained, and at higher P content, the Ni_2P active phase was blocked by excess P. The activity results indicate that on these novel catalysts, the HDN reactions are structure sensitive while the HDS reactions are structure insensitive.

Key Words: **nickel phosphide; XRD; EXAFS; hydrodesulfurization; hydrodenitrogenation.**

INTRODUCTION

Transition metal phosphides have recently been reported as a new class of high-activity hydroprocessing catalysts. Among the phosphides studied, the group 6 compounds, MoP and WP (1–4), have been reported to be more active than sulfides. For the iron group compounds, Fe_2P, CoP, Co_2P, and Ni_2P (5–7), activity has been found to be moderate, with Ni_2P having the highest activity, especially for hydrodenitrogenation. However, these catalysts suffered from a tendency to deactivate with time on stream (5). This paper examines the effect of phosphorus content on the performance of supported Ni_2P/SiO_2. A remarkable effect was observed on increasing the phosphorus content, which greatly increased the activity and stability of the catalysts, making this one of the best performing materials for hydroprocessing.

Phosphorus in the form of phosphate has been investigated and recommended as a secondary promoter in hydroprocessing Co–Mo and Ni–Mo sulfide catalysts over a period of almost 40 years and is used in a number of commercial catalysts (8). Many researchers have studied the effect of phosphorus in sulfide catalysts (9–12), and the topic has been reviewed by Iwamoto and Grimblot (13). An extensive literature reports on various effects of phosphate in the catalysts. Many studies describe a beneficial effect of phosphorus in catalytic activity in hydrodesulfurization (HDS) (14–20), hydrodenitrogenation (HDN) (17–19, 21–24), and hydrogenation (HYD) ability (25–27). In some instances, no improvement in reactivity by phosphorus is reported (28). The results presented in that paper indicated that P added to MoS_2/Al_2O_3 catalysts acted directly on the support to form $AlPO_4$, and it was speculated that weaker interactions of MoS_2 with the support surface increased the stacking of MoS_2 layers. Most studies find an enhancement in activity, however, and offer several explanations for the effect of P. These include stabilization of solutions of high metal concentrations that can yield a more uniform impregnation (29), improvement of the resistance to coking

[1] To whom correspondence should be addressed. E-mail: oyama@vt.edu.

0021-9517/02 $35.00

and increased support strength and stability (30, 31), improvement of the dispersion of the Mo and W active phases (8, 14–16), optimization of acidity (8, 32), formation of a new kind of active site with direct participation of phosphorus (33), and alteration of the reaction mechanism (19, 34, 35). The positive effect of phosphorus depends on the concentration and the method of catalyst preparation and may be negative when these are not properly controlled (8, 19, 25).

Although considerable attention has been placed on understanding the role of phosphorus in Mo- and W-based hydrotreating catalysts, until recently, phosphorus compounds themselves have not been studied in hydroprocessing (1–6). This paper discusses the importance of controlling the amount of phosphorus in the preparation of supported catalysts in order to ensure formation of the active phosphide phase without blocking sites.

EXPERIMENTAL

Materials

The support used in this study was silica (Cabosil, L-90). The chemicals used in the synthesis of the catalysts were $Ni(NO_3)_2 \cdot 6H_2O$ (Aesar, 99%) and $(NH_4)_2HPO_4$ (Aldrich, 99%). The chemicals utilized in the reactivity study were dibenzothiophene (Aldrich, 99.5%), quinoline (Aldrich, 99.9%), benzofuran (Aldrich, 99.9%), tetralin (Aldrich, 99.5%), and tetradecane (Jansen Chimica, 99%). The gases employed were He (Airco, Grade 5, 99.99%), CO (Linde Research Grade, 99.97%), 0.5% O_2/He (Airco, UHP Grade, 99.99%), H_2 (Airco, Grade 5, 99.99%), N_2 (Airco, 99.99%), and 30% N_2/He (Airco, UHP Grade, 99.99%).

Synthesis

A series of novel, high-activity hydroprocessing catalysts (Ni_2P/SiO_2) were successfully prepared by means of temperature-programmed reduction (TPR), keeping the nickel content constant and varying the phosphorus content. The samples prepared had initial Ni/P ratios of 2/1, 1/1, 1/1.8, 1/2, 1/2.2, and 1/3 and are labeled accordingly, even though the principal phase in all samples was Ni_2P. Elemental analysis showed that there was loss of phosphorus during the reduction stage for the higher-phosphorus-content samples. The materials were synthesized in two steps. In the first step, aqueous nickel phosphate solutions were prepared by reacting nickel nitrates with acidified ammonium phosphate and these were used to impregnate silica by the incipient wetness impregnation method. In the second step, these phosphates were reduced to phosphides by the method of temperature-programmed reduction. The preparation of nickel phosphate on silica with an initial Ni/P ratio of 1/1 is presented below to illustrate the process.

Prior to use, the silica was dried at 393 K for 3 h and calcined at 773 K for 6 h. The incipient wetness point of the silica was found to be 2.2 $cm^3\ g^{-1}$. In the fist step of preparation, 3.05 g (23.12 mmol) of $(NH_4)_2HPO_4$ was dissolved in 10 cm^3 of distilled water in a flask to form a transparent colorless solution, and 6.72 g (23.12 mmol) of $(Ni(NO_3)_2 \cdot 6H_2O)$ was then added. The clear solution immediately turned into a light-color mixture with some precipitate. A few drops of nitric acid were added in order to dissolve the precipitate and this resulted in a clear green solution, which was further diluted to a volume of 44 cm^3. The solution was impregnated on 20 g of silica. After impregnation, the powder was dried at 393 K for 3 h and calcined at 773 K for 6 h. The calcined sample was ground with a mortar and pestle, pelletized with a press (Carver, Model C), and sieved to particles of diameter between 650 and 1180 μm. In the second step of preparation, temperature-programmed reduction (TPR) was utilized to convert the phosphate into phosphide. The reduction was carried out in a U-shaped quartz reactor placed in a furnace controlled by a temperature programmer (Omega Model CN 2000). The temperature was monitored by a local chromel-alumel thermocouple placed in a thermowell near the center of the reactor bed. The H_2 flow rate was set at 1000 $\mu mol\ s^{-1}$ (1500 cm^3 of NTP min^{-1}) per g of sample. A portion of the exit gas flow was sampled through a leak valve into a mass spectrometer (Ametek/Dycor Model MA 100), the masses 2 (H_2), 4 (He), 15 (NH), 18 (H_2O), 28 (N_2), 31 (P), 32 (O_2), 34 (PH_3), 44 (CO_2), and 62 (P_2) were monitored during the experiment, and these and the temperature in real time were recorded by an online computer. At the end of the temperature program, the sample was cooled in helium to room temperature and was passivated in a 0.5% O_2/He flow for 2 h.

All other samples were prepared in the same manner, using 20 g of SiO_2, 23.12 mmol of nickel nitrate ($Ni(NO_3)_2 \cdot 6H_2O$), and amounts of ammonium phosphate $(NH_4)_2HPO_4$ ranging from 15.6 to 69.3 mmol for the samples with Ni/P ratios of 2/1–1/3. Though the moles of Ni used were constant, the weight percent of Ni varied from sample to sample because of the variable content of P. For the sample with Ni/P = 1/2 the Ni weight percent was 5.58. This corresponds to a weight loading of Ni_2P of 7.91%.

Characterization

The synthesized materials were characterized by CO chemisorption, N_2 physisorption, X-ray diffraction (XRD), elemental analysis, and extended X-ray absorption fine structure measurements (EXAFS). Irreversible CO uptake measurements were used to titrate the surface metal atoms and to provide an estimate of the active sites on the catalysts. Uptakes were obtained after passivation and rereduction, which is referred to here as *ex situ* chemisorption. Usually, 0.2 g of a passivated sample was loaded into a quartz reactor

and pretreated in H_2 at 723 K for 2 h. After being cooled in He, pulses of CO in a He carrier flowing at 26.7 μmol s^{-1} (40 cm^3 of NTP min^{-1}) were injected at room temperature through a sampling valve and the mass 28 (CO) signal was monitored with a mass spectrometer.

BET surface area measurements were carried out right after the CO uptake determinations, using a similar flow technique. Adsorption at liquid nitrogen temperature was performed using a 30% N_2/He stream, and the desorption area obtained after rapid heating was compared to the area of a calibrated volume (35.4 μmol). The surface area was calculated from the one-point BET equation.

X-ray diffraction (XRD) patterns of both the fresh and spent samples were determined with a Scintag XDS-2000 powder diffractometer operated at 45 kV and 40 mA, using Cu $K\alpha$ monochromatized radiation ($\lambda = 0.154178$ nm). Crystal size, specific surface area, and metal site density were calculated by the methods described elsewhere (5). For quantitative measurements, an amount of 10 wt% vanadium metal was mixed with the samples as an internal standard.

Elemental analysis was carried out with an inductively coupled plasma (ICP) instrument (Spectro Analytical Instruments, Model Spectroflame FTMO A85D) on undried samples that had been dissolved in aqua regia in a microwave digester. The nickel and phosphorus signals were calibrated with a solution of nickel nitrate and ammonium phosphate.

In order to understand the effect of the phosphorus content on the structure of the catalysts, the samples were examined using EXAFS. Nickel *K*-edge EXAFS spectra were obtained for fresh and spent samples with Ni/P ratios of 2/1, 1/2, and 1/3. The low concentration of the active phase on the catalysts made their detailed characterization by X-ray diffraction analysis difficult. The fresh samples were pretreated in H_2 flow at 723 K as for the CO chemisorption measurements and were loaded into glass cells with Kapton windows without exposure to the atmosphere. The cells were glass-blown shut to protect the samples. For the spent catalysts, samples were taken from the hydroprocessing reactors, washed with hexane, and then pretreated in He flow at 723 K before being loaded in the Kapton cells. The measurements were made in transmission mode at the XAS beamline at the LNLS–National Synchrotron Light Laboratory in Campinas, Brazil, with a 1.4-GeV ring energy and a 100- to 150-mA ring current. The monochromator was equipped with a channel-cut Si(111) crystal and the energy resolution was about 3 eV.

An experimental comparison of the EXAFS spectra of the catalysts were made with bulk standards. The standards were Ni_2P (Cerac, 99.5%), NiO (Cerac, 99%), NiS (Cerac, 99.9%), $NiCO_3[Ni(OH)_2] \cdot 4H_2O$ (Aldrich), NiS_2, Ni_3S_5, and $NiPS_3$. The latter three compounds were synthesized by placing stoichiometric amounts of Ni (Aldrich, 99.8%), S (EM Science, 99%), and red P (Aldrich, 99%) fine powders in sealed quartz ampules and heating (1 K/min) to 1073 K and maintaining this temperature for 100 h. XRD confirmed the phase purity of the prepared standards. The EXAFS measurements of the standards were carried out in beamline BL12B at the Photon Factory, Tsukuba, Japan, and in beamline X18B at the Brookhaven National Laboratory. Both were operated at close to 2.5 GeV with a 400-mA ring current.

Reactivity Studies

Hydrotreating activity of the samples was tested in a three-phase, packed-bed reactor operated at 3.1 MPa and 643 K for hydrodenitrogenation (HDN), hydrodesulfurization (HDS), and hydrogenation (HYD) with a model petroleum liquid containing 2000 ppm nitrogen (quinoline), 3000 ppm sulfur (dibenzothiophene), 500 ppm oxygen (benzofuran), 20 wt% aromatics (tetralin), and balance aliphatics (tetradecane). The schematic of the testing system is shown elsewhere (36). Briefly, the testing unit consisted of three parallel reactors immersed in a fluidized sand bath (Techne, Model SBL-2). The temperature of the reactors was controlled by a temperature controller (Omega, Model 6051). The reactors were 19 mm/16 mm o.d/i.d. 316 SS tubes with a central thermocouple monitoring the temperature of the catalyst bed. The catalysts were in the form of pellets (16/20 mesh) and were supported between quartz wool plugs in a 13-mm-i.d. 316 stainless steel basket. The hydrogen flow rate was set to 100 μmol s^{-1} (150 cm^{-3} of NTP min^{-1}) with a mass flow controller (Brooks, Model 5850E), and the feed liquid flow rate (5 cm^{-3} h^{-1}) was metered from burettes by high-pressure liquid pumps (LDC Analytical, Model NCI 11D5). Quantities of catalysts loaded in the reactor corresponded to the same amount of *ex situ* CO uptake (70 μmol). Prior to reactivity measurements, the catalyst samples were pretreated in exactly the same manner as for the *ex situ* CO uptake measurements. Hydrotreating samples were collected every 2 or 3 h in sealed septum vials and were analyzed off line with a gas chromatograph (Hewlett–Packard, 5890A) equipped with a 0.32 mm i.d. × 50 m fused silica capillary column (CPSIL-5CB, Chrompack, Inc.) and a flame ionization detector. The product of dibenzothiophene HDS was primarily biphenyl. The products of quinoline reaction were the denitrogenated molecules propylbenzene and propylcyclohexane, and the N-containing species, 1,2,3,4-tetrahydroquinoline, 7,8,9, 10-tetrahydroquinoline, and propylaniline. The production of the latter is referred to as HDA. The product of benzofuran reaction was exclusively ethylbenzene, and the production of this product is referred to as HDO.

RESULTS AND DISCUSSION

Ni_2P (37) adopts the hexagonal Fe_2P structure (space group, $P\bar{6}2m$, D^2_{3h}; Struckturbericht notation, revised C22) with lattice parameters $a = b = 0.5859$ nm, $c = 0.3382$ nm.

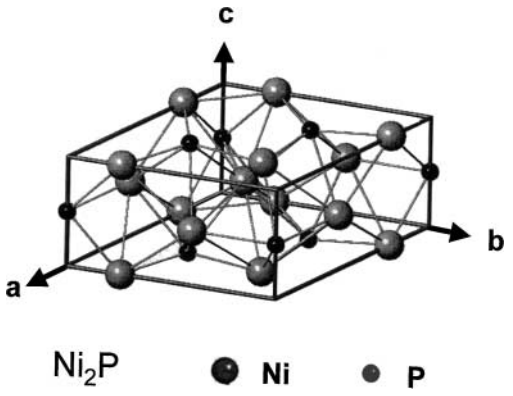

FIG. 1. Crystal structure of Ni_2P.

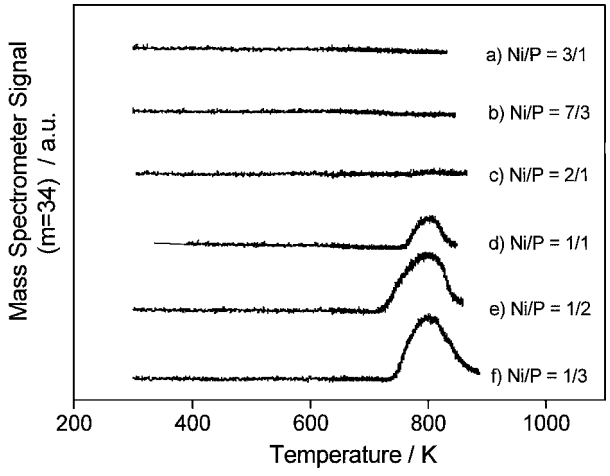

FIG. 3. Mass 34 (PH_3) signal from temperature-programmed reduction of the samples at $\beta = 1$ K/min (0.01667 K s^{-1}). The Ni/P ratios indicated are initial values.

The crystal structure (Fig. 1) and lattice parameters can be used to calculate a bulk density ($\rho = 7.09$ g cm^{-3}) and the average surface metal atom density ($\bar{n} = 1.01 \times 10^{15}$ atoms cm^{-2}) of the solids (5).

The preparation of the supported phosphides was carried out in two stages. First, a solution of the metal and phosphorus components was impregnated on the carrier silica support and the material was dried and calcined to form supported phosphates. Second, the phosphates were transformed into phosphides by temperature-programmed reduction (TPR) (Figs. 2 and 3). Only results for mass 18 (H_2O) and 34 (PH_3) are shown, as the other monitored masses were featureless or provided no additional information. The results for the samples with Ni/P ratios of 1/1.8 and 1/2.2 are not presented in the figures since they were similar to those of the sample with a Ni/P ratio of 1/2.

The TPR traces of mass 18 showed two systematic trends for the samples with different Ni/P ratios. First, for lower P contents (Figs. 2a–2c), the TPR traces showed more peaks and a more complicated overall reduction pattern than that of higher P samples (Figs. 2d–2f). Second, for higher P contents, all the reduction peaks, including the initial and final features, were shifted to higher temperatures. These trends are reasonable. For lower P contents, the precursor probably contains more nickel compounds, such as nickel oxide and nickel oxy-phosphates, and their separate reduction results in different peaks. Since nickel oxides are easily reducible, the TPR peaks appear at lower temperatures. It is possible that some metallic Ni or a nickel phosphide phase of lower P content was formed which assisted the reduction of other species. For higher P contents (Figs. 2d–2f), the nickel is likely to be in the form of phosphate and reaction occurs at the high intrinsic reduction temperature, T_p, of this main phosphate phase. As can be seen from Figs. 2d–2f, the peak temperature of the reduction traces was around 800 K and was characteristic of the reduction of bulk nickel phosphate (5). Because this temperature was high, successive reduction stages could not be resolved, and the whole process appeared to occur in one step. It should be noted that in these TPR measurements there was an inadvertent change in heating rate at ~630 K. This resulted in a drop in intensity, especially for Figs. 2a–2c, but it does not affect the interpretation of the data.

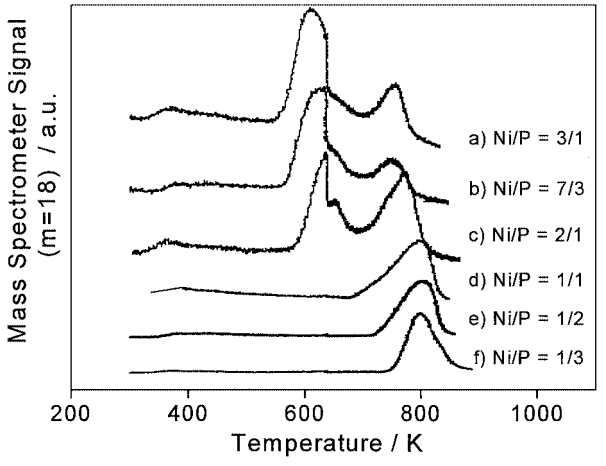

FIG. 2. Mass 18 (H_2O) signal from temperature-programmed reduction of the samples at $\beta = 1$ K/min (0.01667 K s^{-1}). The Ni/P ratios indicated are initial values.

The TPR trace for mass 31 (P) followed exactly that of mass 34 (PH_3) and is not reported here. It is likely that the P observed was a fragmentation product of PH_3. The trace for mass 62 (P_2) was completely flat and suggests that elemental phosphorus was not volatilized from the sample.

As will be discussed shortly, the major phase seen in all the samples was Ni_2P, so the stoichiometric ratio was Ni/P = 2/1. It was observed that only the samples prepared with phosphorus in excess of this stoichiometry showed loss of P during the synthesis. This is seen in the production of PH_3 in increasing amounts in the TPR traces for the samples with initial Ni/P ratios of 1/1, 1/2, and 1/3 (Fig. 3). For

TABLE 1

Catalyst Characterization Results

Initial sample Ni/P ratio	Sample	Surface area, S_g ($m^2\ g^{-1}$)	CO uptake ($\mu mol\ g^{-1}$)	Metal site density ($\mu mol\ g^{-1}$)	D_c (nm)
2/1	Fresh	90	49	42	26
	Spent	107	18	42	26
1/1	Fresh	98	15	67	20
	Spent	100	13	67	20
1/1.8	Fresh	111	24	150	11
	Spent	110	14	150	11
1/2	Fresh	97	28	170	9
	Spent	89	24	170	9
1/2.2	Fresh	106	27	190	9
	Spent	103	30	190	9
1/3	Fresh	100	32	310	7
	Spent	75	16	310	7

the samples with lower P contents, no P or PH_3 was evolved during the reduction.

The BET specific surface areas (S_g) and CO chemisorption uptakes of the samples are listed in Table 1. The specific surface areas (S_g) of the samples were close to that of the support (90 $m^2\ g^{-1}$). Deviations were due to experimental error with the flow technique. The experimental CO uptakes of the samples are reported in the fourth column of Table 1. The fresh sample prepared with initial Ni/P ratio of 2/1 had the highest CO uptake (49 $\mu mol\ g^{-1}$), while the rest of the samples had uptakes between 15 and 32 $\mu mol\ g^{-1}$. Other fresh samples were all close. The crystallite sizes (D_c) calculated from the Scherrer equation ($D_c = K\lambda/\beta\cos\theta$) (38) are listed in the last column of Table 1. The analysis shows that crystallite size gets smaller with an increase in P content. From the crystallite size, it is possible to calculate an effective surface area ($S = 6/\rho D_c$) of the crystallites assuming cubic or spherical geometry, and from this a theoretical metal site concentration, (L). This surface concentration is given by $(L) = S\bar{n}f$, where f is the fractional weight loading of the sample and $\bar{n}$ is again the average surface metal atom density, which for Ni_2P is 1.01×10^{15} atoms cm^{-2} (5). The results are listed in the fifth column of Table 1 and show that the metal site concentration increases with an increase in the P content in the samples. In fact, however, the CO uptakes for the fresh samples starting with the sample with an initial Ni/P ratio of 1/1 increase only slightly with P content. This indicates that the extra phosphorus is possibly blocking sites. This is discussed below.

X-ray diffraction patterns of the fresh samples prepared with initial Ni/P ratios of 2/1, 1/1, 1/2, and 1/3 are presented in Fig. 4. Here, again, the patterns for the samples prepared with initial Ni/P ratios of 1/1.8 and 1/2.2 are not shown in the figure since they were similar to the one for Ni/P = 1/2. The diffraction patterns displayed two systematic features. First,

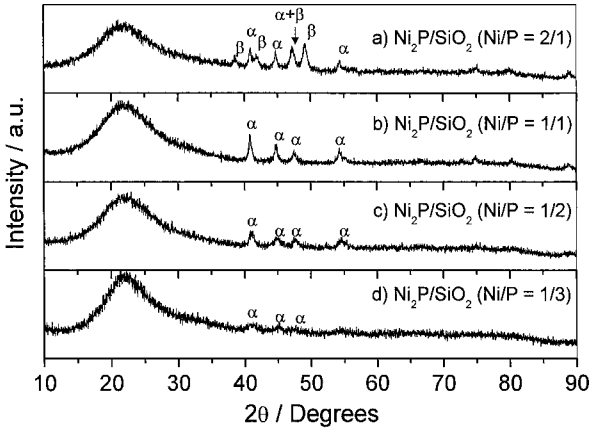

FIG. 4. X-ray diffraction patterns of the fresh samples (α, Ni_2P; β, $Ni_{12}P_5$). The Ni/P ratios indicated are initial values.

the sample with the lowest P content (Fig. 4a) contains two phases (Ni_2P and $Ni_{12}P_5$) in the product, while the samples with the higher P contents had just one phase, Ni_2P. The formation of $Ni_{12}P_5$ at lower P content is understandable, as $Ni_{12}P_5$ contains a lower proportion of P than does Ni_2P. Second, the X-ray diffraction peaks became less intense and weaker with increasing content of P. The linewidth indicates the formation of smaller crystallites of Ni_2P with an increase in P content, as is shown in the last column in Table 1, and is a likely consequence of a greater dispersion of the precursor phosphate, which is easier to form with higher P contents. It may be that the Ni component is able to spread itself more during the calcination stage with larger amounts of phosphate on the surface.

X-ray diffraction patterns were also obtained for the spent samples (Fig. 5, upper curve in each frame). The figure shows that there was no change in pattern for the sample

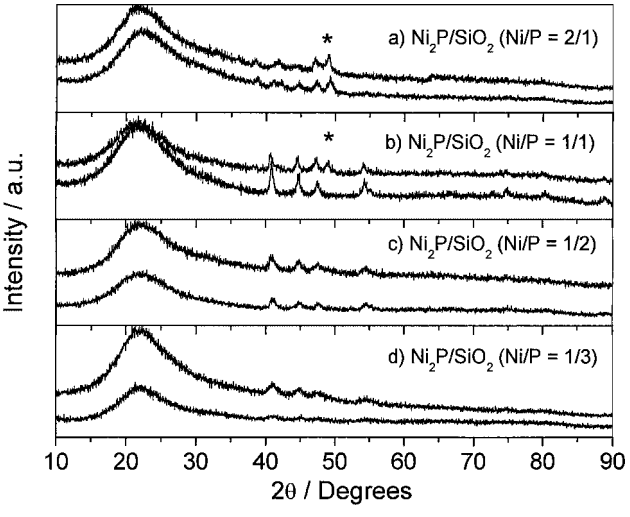

FIG. 5. Comparison of X-ray diffraction patterns for the fresh samples and the spent samples. The Ni/P ratios indicated are initial values.

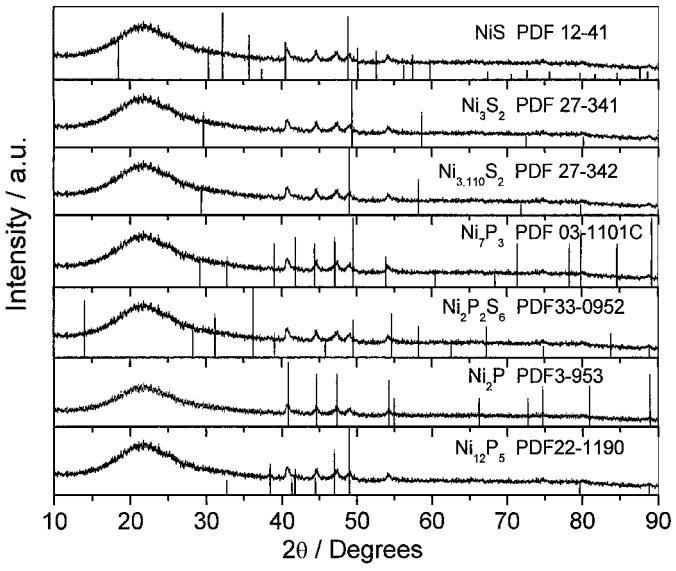

FIG. 6. Superposition of the X-ray diffraction pattern of the spent Ni_2P/SiO_2 sample (Ni/P = 1/1) with different references. The Ni/P ratio is an initial value.

with an initial Ni/P ratio of 2/1 (Fig. 5a), indicating that the Ni_2P and $Ni_{12}P_5$ were stable phases at hydrotreating conditions. For the samples with initial Ni/P ratios of 1/2 and 1/3, the nickel phosphide phase became more crystallized after the hydrotreating reaction (Figs. 5c and 5d). This is understandable due to the prolonged exposure (>100 h) to the hydrotreating temperature of 643 K. For the sample with an Ni/P ratio of 1/1 (Fig. 5b), the X-ray diffraction pattern after reaction shows the appearance of a new peak, which is assigned to $Ni_{12}P_5$. The basis for the assignment to $Ni_{12}P_5$ is shown in Fig. 6, which superposes the pattern for the spent sample with an initial Ni/P = 1/1 ratio on the other nickel phosphide, nickel sulfide, and nickel phosphide sulfide PDF reference patterns. The main peaks belong to Ni_2P, but all the minor features match well those of $Ni_{12}P_5$ (bottom pattern). It is likely that the Ni_2P in this sample was slightly phosphorus deficient to start out with, and the prolonged exposure to the reaction temperature caused the $Ni_{12}P_5$ to nucleate. It is also possible that the sample lost some phosphorus during reaction, though this is less likely, as it was not observed with the other samples.

Table 2 presents elemental analysis results for representative samples. The sample prepared with an initial Ni/P ratio of 2/1 showed after reaction a Ni/P ratio of 1/0.46, which was close to the expected value of 1/0.50. The small deficiency in P is consistent with the observation of $Ni_{12}P_5$ coexisting with Ni_2P in this sample. The sample with an initial Ni/P ratio of 1/2 showed after calcination a Ni/P ratio of 1/2.03, which was close to the initial value. Thus, no phosphorus was lost in the calcination stage. After reaction, the same sample showed a ratio of 1/0.57, which was close to the expected value for Ni_2P of 1/0.50. Despite the fact that this sample was prepared with a threefold excess of phosphorus, the final catalyst contained just over the stoichiometric amount of P. Most of the extra P was probably lost in the high-temperature reduction step, as shown by its TPR trace (Fig. 3e). We cannot determine where the phosphorus resides or in what oxidation state. Most of it is likely to be on the support as unreduced phosphate, but part is possibly on the surface of the Ni_2P crystallites as phosphide, as the CO uptake (Table 1) is smaller than the theoretical number of surface metal atoms. A similar result was found for the sample with an initial Ni/P ratio of 1/3. The final catalyst after reaction showed a Ni/P ratio of 1/0.75, which represents a much smaller P content compared to the initial composition. There was still substantial excess P, and most of it was probably located on the support surface as unreduced phosphate. The remaining P probably resided on the surface of the Ni_2P crystallites, as seen from the blockage of CO adsorption sites for this sample (Table 1).

The question arises as to the existence of an amorphous nickel phosphide phase in conjunction with the crystallites. Such phases have been reported (39) but are not likely to be major here. Reviewing the results presented in Table 1, it can be seen that the CO uptake values are below the theoretical surface metal site density for all samples. If the experimental values had been higher, then such an amophous phase might have been indicated, as it likely would have contributed to the CO uptake. Of course, it could be that the sites on this phase are blocked by extra phosphorus, but then they would be unreactive, so it would not affect the conclusions on reactivity.

To check on the possibility of the presence of an amorphous phase, a quantitative XRD experiment was carried out on the fresh Ni_2P/SiO_2 with an initial Ni/P ratio of 1/2. The results are shown in Fig. 7. A sample consisting of a physical mixture of Ni_2P and SiO_2 (Fig. 7a) of the same loading is compared to a sample of the Ni_2P/SiO_2 (Fig. 7b), utilizing an internal reference consisting of 10 wt% V metal. The 10% V metal (Fig. 7c) was chosen because according to its PDF standard (Fig. 7d) its XRD lines do not interfere with those of Ni_2P (Fig. 7e). From the integrated peak intensities, the Ni_2P content of the supported sample is found to be 90% of the reference sample. The comparison of the intensities is not exact because of the different crystallite sizes of the samples, and we estimate an error of 10% in

TABLE 2

Elemental Analysis Results

Initial sample Ni/P ratio	Sample	Ni (wt%)	P (wt%)	Experimental Ni/P ratio
2/1	Spent	5.38	1.29	1/0.46
1/2	Calcined	5.01	5.45	1/2.03
1/2	Spent	5.45	1.65	1/0.57
1/3	Spent	5.67	2.23	1/0.75

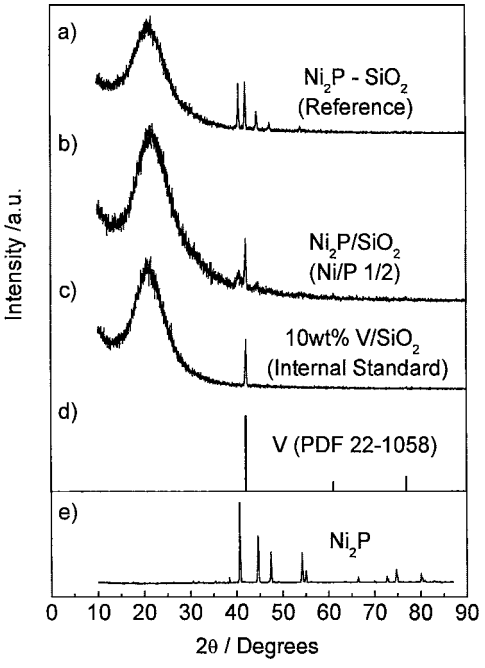

FIG. 7. Quantitative X-ray diffraction analysis of Ni_2P/SiO_2. (a) Physical mixture of Ni_2P–SiO_2 with 10 wt% V as internal standard. (b) Freshly reduced Ni_2P/SiO_2 sample (initial Ni/P = 1/2) with 10 wt% V as internal standard. (c) Physical mixture of 10 wt% V and SiO_2. (d) PDF file for metallic vanadium. (e) Bulk Ni_2P standard.

this determination. The conclusion is that if an amorphous phase is present, it is a minority phase accounting for only about 10% of the nickel content. Evidence from EXAFS spectra to be discussed shortly indicate that the Ni–Ni and Ni–P distances in the fresh catalyst samples are the same as in crystalline Ni_2P, again indicating the absence of a substantial amorphous phase.

Figures 8 and 9 present the time course of HDS and HDN activities on the series of phosphide catalysts. Figure 10

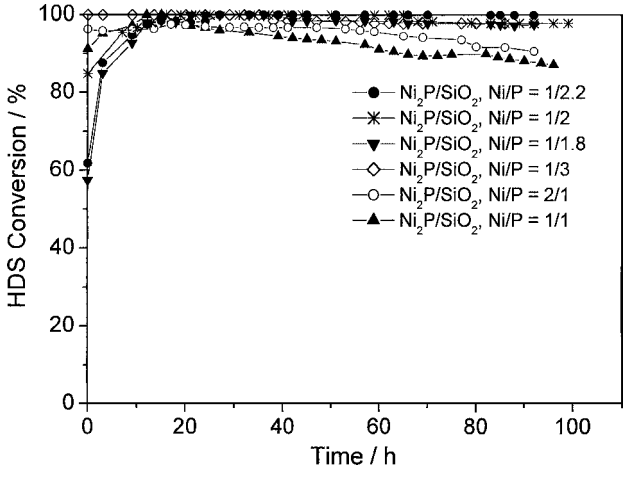

FIG. 8. Hydrodenitrogenation performance of supported catalysts. The Ni/P ratios indicated are initial values.

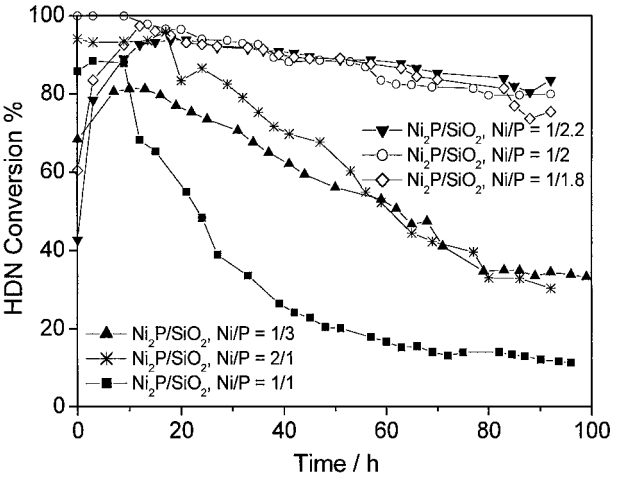

FIG. 9. Hydrodesulfurization performance of supported catalysts. The Ni/P ratios indicated are initial values.

shows the effect of phosphorus content on the HDS and HDN activities. The HDS activity was uniformly high for all the samples, with just slight reductions for the samples with initial Ni/P ratios of 2/1 and 1/1. The sample with an initial Ni/P ratio of 1/2.2 had the highest HDS conversion, essentially 100%, although the other three samples, with initial Ni/P ratios of 1/1.8, 1/2, and 1/3, had the very close HDS conversion of 98%. The small effect of the P content was close to the error in the measurements of 1–2%, but the trends are probably real, as shown more clearly in the HDN reactions. In fact, the samples with initial Ni/P ratios of 1/1.8 and 1/2.2 were prepared and tested to confirm the high-activity results of the sample with an initial Ni/P ratio of 1/2.

The product distribution and conversions obtained with the various catalysts are summarized in Table 3. The result of reaction of dibenzothiophene was exclusively the HDS

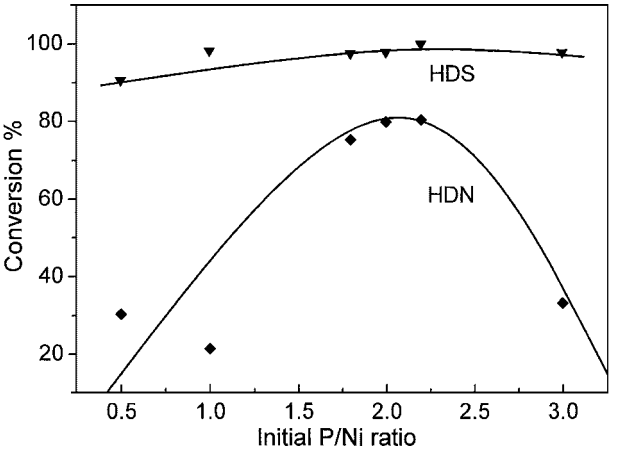

FIG. 10. Comparison of hydroprocessing activities. The P/Ni ratios indicated are initial values.

TABLE 3

Conversions and Product Distributions[a]

Reactants	Ni/P	Conversion (%) 2/1	1/1	1/1.8	1/2	1/2.2	1/3	Product	Selectivity (%) 2/1	1/1	1/1.8	1/2	1/2.2	1/3
Dibenzothiophene	HDS	90.6	98.3	97.6	97.9	100	97.9	Biphenyl	100	100	100	100	100	100
Quinoline	HDN	30.4	21.5	75.4	79.9	80.4	33.3	Propylcyclohexane	15.0	4.1	37.1	50.0	48.9	7.9
								Propylbenzene	14.7	8.8	39.8	27.6	33.2	25.7
	HYD	45.4	44	17.4	19.5	16.0	33.2	5,6,7,8-Tetrahydroquinoline	21.0	32.6	5.8	3.9	4.7	16.1
								Orthopropylaniline	38.8	30.9	13.4	14.7	10.8	39.7
								1,2,3,4-Tetrahydroquinoline	10.5	23.6	3.8	3.7	2.3	10.6
Benzofuran	HDO	21.6	35.0	49.5	46.0	64.0	81.0	Ethylbenzene	100	100	100	100	100	100
Tetralin	De-HYD	19.4	31.3	48.6	22.6	27.3	54.7	Naphthalene	96.9	98.2	98.4	94.9	96.6	99.1
	HYD	0.6	0.6	0.8	1.2	1.0	0.5	*trans*-Decalin	1.2	0.6	0.9	2.7	1.9	0.3
								cis-Decalin	1.9	1.2	0.7	2.4	1.5	0.6

[a] Catalyst loading based on 70-μmol CO uptake.

product biphenyl. The absence of hydrogenated intermediates indicates that the pathway for HDS may be direct sulfur removal. The results of reaction of quinoline were different, showing both HDN and HYD products. The HDN products were propylcyclohexane and propylbenzene, and the HYD products were 5,6,7,8-tetrahydroquinoline, orthopropylaniline, and 1,2,3,4-tetrahydroquinoline. The most active catalysts produced greater amounts of HDN products with higher propylcyclohexane than propylbenzene. This indicates that hydrogenation as well as nitrogen scission are important in the total HDN reaction. The product of benzofuran reaction was exclusively the HDO product ethylbenzene. HDO is a facile reaction compared to HDS and HDN and probably does not interfere with the S- and N-removal reactions. The product of tetralin reaction was mostly the dehydrogenation product naphthalene, with some *cis*- and *trans*-decalin also formed. This is the expected product distribution from thermodynamics.

For the HDN reaction, the P content had a strong effect on the quinoline reaction. The samples with initial Ni/P ratios of 1/1.8, 1/2, and 1/2.2 followed similar time courses with slight deactivation, resulting in final HDN conversions between 80 and 90% (Fig. 9). The other three samples reached a far lower HDN activity, which was below 50%, especially for the highest and lowest P content samples. A comparison of all results is presented in Fig. 10, which shows the effect of P content on the activity of all the catalysts. The best performance was obtained at an initial Ni/P ratio close to 1/2.

The effect of P content on HDS and HDN on these samples gives insight into the nature of the active sites responsible for these reactions. In the case of HDS the small effect of P content on conversion suggests that the reaction occurs principally on metal centers and that there is little effect of ensemble size on reactivity. Hence, the reaction is structure insensitive. The reaction may occur by direct sulfur removal from dibenzothiophene, as no hydrogenated intermediates are observed.

In contrast, in the case of HDN, the relatively large effect of P on conversion suggests that P somehow participates in the reaction. The HDN of quinoline does not occur directly because of the greater strength of the C–N bonds and is a complex sequential reaction involving hydrogenation of the N-ring, hydrogenolysis of the aliphatic C–N bond (CNH), hydrogenation of the C6-ring (HYD), and elimination of ammonia. On sulfides detailed kinetic studies show that the rates of HYD and CNH are of a similar order of magnitude, and no single rate-limiting step is operative (40, 41). On phosphides such studies have not been carried out, but it is likely that again no single rate-limiting step is involved, and that CNH will be one of the key steps. The CNH reaction is a complex reaction and requires multiple sites (42–45), among them an acid site to bind the nitrogen compound and a proximal basic site to carry out a β-H attack. Thus, the reaction is structure sensitive. Changes of P levels on the surface may disrupt the dual site and cause the observed maximum in activity with P content. The phosphidic P^{3-} may act as a base, in a manner similar to sulfidic S^{2-}, and assist in abstracting a proton from the adsorbed nitrogen-ring intermediate.

Previous work had shown that Ni_2P/SiO_2 (initial Ni/P = 1/1) was only a fair catalyst for hydroprocessing, especially for hydrodesulfurization (HDS) of dibenzothiophene (5). Also, the HDN activity declined considerably with time. In this work, the addition of excess phosphorus is seen to facilitate the formation of the active nickel phosphide phase, and to reduce deactivation.

The CO uptake for the posthydrotreating samples decreased for all samples except for the sample with a Ni/P ratio of 1/2.2. This fact was more obvious for the samples with the lower P contents, as is shown in Table 2. For example, the CO uptake of the fresh sample with the Ni- to-P ratio of 2/1 was 49 μmol g^{-1}, but it decreased to 18 μ mol g^{-1} after the hydrotreating. This loss of active centers may be an important reason for the deactivation of the catalysts.

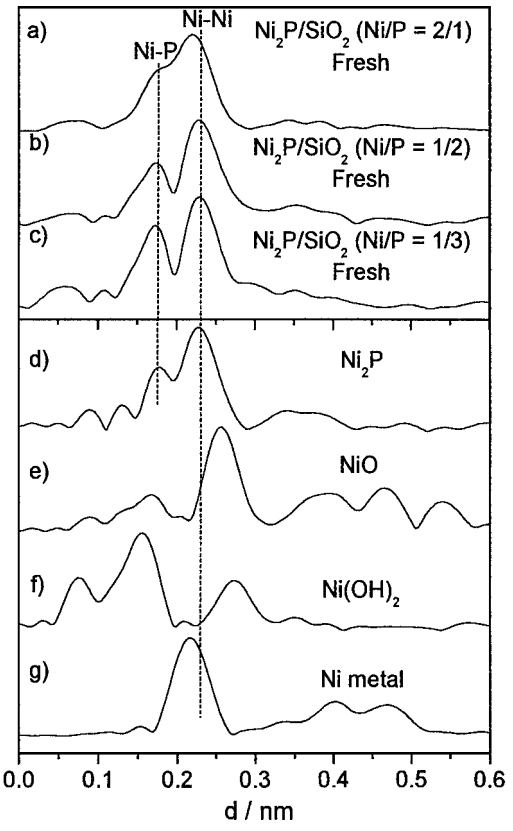

FIG. 11. Comparison of nickel *K*-edge EXAFS for the fresh samples with Ni/P ratios of (a) 2/1, (b) 1/2, and (c) 1/3 and for references (d) Ni_2P, (e) NiO, (f) $Ni(OH)_2$, and (g) Ni metal. The Ni/P ratios indicated are initial values.

In order to better understand the effect of the phosphorus content on the catalytic activity, the catalysts were examined using extended X-ray absorption fine structure (EXAFS) analysis. The top panel in Fig. 11 shows the Ni *K*-edge EXAFS results for these fresh samples prepared with initial Ni/P ratios of 2/1, 1/2, and 1/3. The sample with initial Ni/P = 2/1 (Fig. 11a) shows a main peak with a shoulder at lower interatomic distance. In contrast, the samples with initial Ni/P = 1/2 and 1/3 (Figs. 11b and 11c) display two distinct peaks. Comparison of the latter with the reference Ni_2P sample shows good agreement in the Ni–Ni and Ni–P distances. There is no such agreement with the features of NiO, $Ni(OH)_2$, or Ni metal, and this demonstrates that the predominant phase in these two supported catalysts is Ni_2P. The situation is different for the sample with the initial Ni/P ratio of 2/1 (Fig. 11a). In this case the Ni–P peak is reduced to a shoulder and the Ni–Ni peak shifts to the position of metallic Ni. It is evident that the amount of Ni_2P phase is smaller, as could be expected from the spreading of the metal and phosphorus components on the surface of the support. The lack of the Ni_2P also explains the low activity. With the Ni_2P/SiO_2 sample with the excess phosphorus (initial Ni/P = 1/3), the FT peak positions duly correspond to those of bulk Ni_2P. However, the intensity of the Ni–P relative to the Ni–Ni peak is now increased over that of bulk Ni_2P. The extra phosphorus probably resides on the surface of the highly dispersed particles, breaking up the catalytically active ensembles and again reducing activity.

Figure 12 compares the EXAFS spectra of the fresh and spent samples with initial Ni/P ratios of 2/1, 1/2, and 1/3. In all cases changes can be discerned in the catalysts after reaction. For the spent sample with initial Ni/P = 2/1, a small feature appears between the main Ni–Ni peak and the Ni–P shoulder (Fig. 12a). For the spent sample with initial Ni/P = 1/2, the two-peak structure is retained, but there is a reduction in the Ni–Ni peak intensity (Fig. 12b). For the spent sample with initial Ni/P = 1/3, the Ni–Ni peak is almost entirely attenuated and a broad feature at lower interatomic distance appears (Fig. 12c). Clearly, in all cases there is disruption of the original Ni_2P phase, and this is likely due to the formation of sulfur compounds. Nickel carbide and nickel nitride are unstable at the conditions of reaction (46). The identification of the changes occurring in the spent samples was carried out by comparing their spectra to those of bulk sulfide references (Fig. 13).

For the spent sample with initial Ni/P = 2/1 (Fig. 13a), the small feature between the Ni–Ni peak and the Ni–P shoulder corresponds to a Ni–S distance in one of the sulfide

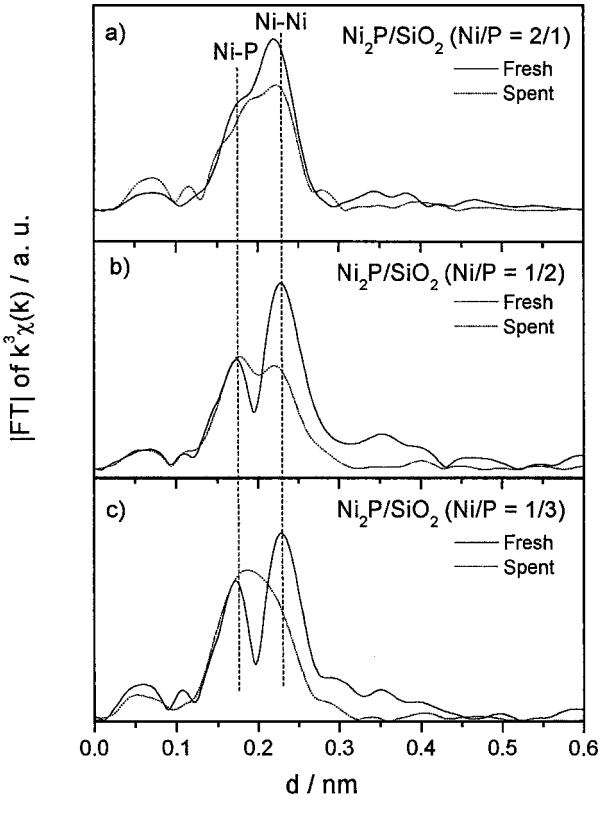

FIG. 12. Nickel *K*-edge EXAFS of the fresh and spent samples with different Ni/P ratios: (a) Ni/P = 2/1, (b) Ni/P = 1/2, and (c) Ni/P = 1/3. The Ni/P ratios indicated are initial values.

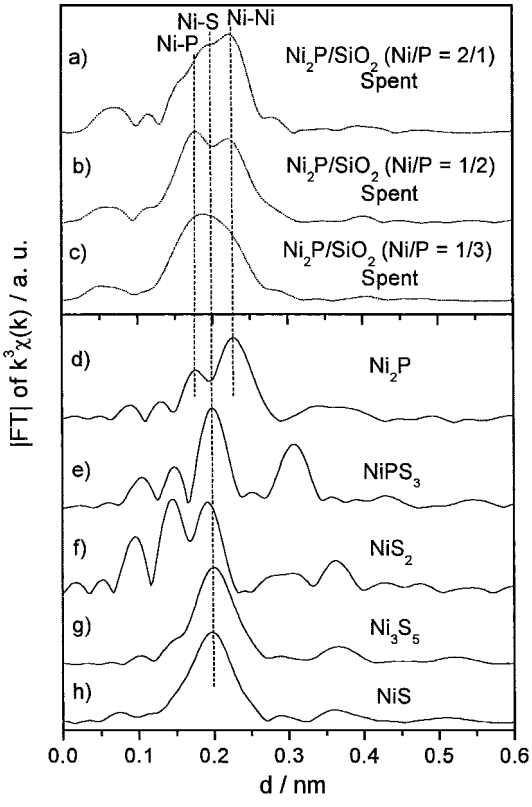

FIG. 13. Comparison of nickel *K*-edge EXAFS for the spent samples with Ni/P ratios of (a) 2/1, (b) 1/2, and (c) 1/3 and for references (d) Ni_2P, (e) $NiPS_3$, (f) NiS_2, (g) Ni_3S_5, and (h) NiS. The Ni/P ratios indicated are initial values.

references (Figs. 13e–13h). The distance is similar to the Ni–S distance in materials such as NiS_2, Ni_3S_5, and NiS, and the observed signal matches this, but no longer distance appears as in $NiPS_3$ (Fig. 13e). It is interesting that the sample now shows Ni–Ni and Ni–P distances that correspond to Ni_2P whereas the fresh sample showed distances displaced toward Ni metal. It is likely that the metallic portion of this sample was sulfided, but that the phosphide portion was retained.

For the spent Ni_2P/SiO_2 sample with initial Ni/P = 1/2 (Fig. 13b), a two-peak spectrum with the characteristic distance of Ni_2P (Fig. 13d) is visible. However, peaks are broadened in comparison to the fresh sample (Fig. 11b) and the Ni–Ni peak is attenuated. It is likely that if a Ni–S signal is present it is hidden between the two peaks, broadening the spectra and reducing the Ni–Ni contribution. Still, the main features of the Ni_2P remain and the conclusion is that the active phase is a surface phosphosulfide. It is unlikely to be a high-sulfur phase like $NiPS_3$, as the strong feature at long interatomic distance is missing.

For the spent Ni_2P/SiO_2 (initial Ni/P = 1/3), the spectrum consists of a broad feature that is likely formed from a combination of different peaks. The most likely interpretation is that there is a dominant Ni–S signal and smaller peaks due to Ni–P and Ni–Ni on both sides. It is difficult to understand why this sample should undergo greater sulfidation than the sample with initial Ni/P = 1/2, as it contained more phosphorus in the fresh state. However, recalling the XRD results (Fig. 5) that showed the sample with initial Ni/P = 1/3 to be more highly dispersed than the sample with initial Ni/P = 1/2, it can be conjectured that the smaller particle size results in a greater degree of sulfidation.

The characterization of the P and S components by direct EXAFS or X-ray absorption near-edge spectroscopy (XANES) measurements was not possible with our current capabilities because the low energy of their *K*- and *L*-edge transitions required windowless operation and exposure to air. Thus, the conclusions above about the surface compositions of the materials are tentative. However, measurements of the XANES at the Ni-edge of both the freshly reduced and the spent catalysts showed that they were all in the metallic range (8340–8343 eV), indicating that metal phosphides were the predominant phases, in agreement with the interpretation presented. It can be deduced that the P and S components associated with Ni are not oxidized.

The catalytic testing showed that the activity of the phosphides was uniformly high for HDS but went through a maximum with P content for HDN (Fig. 10). Separate tests with NiS_2/SiO_2 showed that it has very low activity in both HDS and HDN, in agreement with results from the literature (47). These results indicate that in the supported Ni_2P/SiO_2 sample the phosphorus plays an important role in the catalytic phase and supports the conclusion that Ni–P bonding is present in all the spent samples, even though a substantial amount of Ni–S bonding is seen in the spectra. The best sample Ni_2P/SiO_2 (initial Ni/P = 1/2) represents an optimum where the phosphorus content and the particle size are balanced to give some sulfur tolerance with the maintenance of high catalytic activity.

The significant finding of this study was the very high activity of the nickel phosphide catalysts prepared with initial Ni/P ratios close to 1/2 (the final ratio was close to stoichiometric Ni_2P, Ni/P = 1/0.57). The sample with the initial Ni/P ratio of 1/2.2 had 100% HDS and 81% HDN conversion, which is much higher than that of a commercial catalyst, Ni–Mo–S/Al_2O_3 (Shell 324), with 76% HDS and 38% HDN (48). This is the highest activity which has been reported in the hydrotreating field for dibenzothiophene in the presence of a nitrogen compound.

CONCLUSIONS

Phosphorus content has a profound effect on the structure and activity of Ni_2P/SiO_2 catalysts. Samples prepared with initial ratios of Ni/P $\approx$ 1/2 result in a material with close to stoichiometric proportions of P (Ni/P = 1/0.5) with excellent activity in hydroprocessing. The samples have an HDS conversion of 100% and HDN conversion of 81%,

which are much higher than those of a commercial Ni–Mo–S/Al_2O_3 catalyst, with HDS conversion of 76% and HDN conversion of 38%, based on the loading in the reactor of 70 μmol of sites titrated by chemisorption. Phosphorus content has a small effect on HDS, indicating that the reaction is structure insensitive, but a substantial one on HDN, indicating that the reaction is demanding. Characterization of the catalysts by EXAFS measurements before and after reaction indicates that the active phase in the catalysts is a phosphosulfide. The catalysts inactive for HDN, on the other hand, have pronounced sulfur content. Overall results indicated that on these novel, high-activity hydroprocessing catalysts, the HDS and HDN reactions are not promoted by nickel on its own, but that phosphorus plays an important role in the reaction.

ACKNOWLEDGMENTS

We acknowledge support from the U.S. Department of Energy, Office of Basic Energy Sciences, through Grant DE-FG02-963414669, from the NEDO International Joint Research Program, and from CONICET, Argentina, through Grant PEI-0132/98. We also acknowledge use of the XAS beamline at the LNLS (National Synchrotron Light Laboratory) in Campinas, Brasil, under Project XAS 592/99 of beamline BL12B at the Tsukuba Photon Factory of the High Energy Accelerator Research Organization under Grant 2001G297, and beamline X18B at Brookhaven National Laboratory under Grant 4513. We also thank J. M. Ramallo-López for assistance in taking data at the SXS beamline.

REFERENCES

1. Li, W., Dhandapani, B., and Oyama, S. T., *Chem. Lett*. 207 (1998).
2. Phillips, D. C., Sawhill, S. J., Self, R., and Bussell, M. E., *J. Catal.* **207**, 266 (2002).
3. Stinner, C., Prins, R., and Weber, Th., *J. Catal*. **191**, 438 (2000).
4. Clark, P., Wang, X., and Oyama, S. T., *J. Catal*. **207**, 256 (2002).
5. Wang, X., Clark, P., and Oyama, S. T., *J. Catal*., in press.
6. Stinner, C., Prins, R., and Weber, Th., *J. Catal*. **202**, 187 (2001).
7. Robinson, W. R. A. M., van Gestel, J. N. M., Koranyi, T. I., Eijsbouts, S., van der Kraan, A. M., van Veen, J. A. R., and de Beer, V. H. J., *J. Catal*. **161**(2), 539 (1996).
8. Lewis, J. M., Kydd, R. A., Boorman, R. M., and Van Rhyn, P. H., *Appl. Catal. A* **84**, 103 (1992).
9. Jian, M., Rico Cerda, J. L., and Prins, R., *in* "Vth Workshop on Hydrotreating Catalysis, European Section, Lille, Villeneuve d'Ascq," p. 225, 1995.
10. Jian, M., and Prins, R., *Catal. Lett*. **35**, 193 (1995).
11. Atasanova, P., Tabakova, T., Vladov, Ch., Halachov, T., and Lopez Agudo, A., *Appl. Catal. A* **161**, 105 (1997).
12. Mangnus, P. J., Van Veen, J. A. R., Eijsbouts, S., De Beer, V. H. J., and Moulijn, J. A., *Appl. Catal*. **61**, 99 (1990).
13. Iwamoto, R., and Grimblot, J., *Adv. Catal*. **44**, 417 (1999).
14. Lewis, J. M., and Kydd, R. A., *J. Catal*. **136**, 478 (1992).
15. Morales, A., and de Agudelo, R., *Appl. Catal*. **23**, 23 (1986).
16. Atanasova, P., Vchyti, J., Kraus, M., and Halachev, T., *Appl. Catal*. **65**, 53 (1990).
17. Cruz Reyes, J., Avalos-Boria, M., López Cordero, R., and López Agudo, A., *Appl. Catal. A* **120**, 147 (1994).
18. van Veen, J. A. R., Colijn, H. A., Hendriks, P. A. J. M., and van Weisenes, A. J., *Fuel Process. Technol.* **35**, 137 (1993).
19. Eijsbouts, S., van Gestel, J. N. M., van Veen, J. A. R., de Beer, V. H. J., and Prins, R., *J. Catal*. **35**, 137 (1991).
20. Fitz, C. W., and Rase, H. F., *Ind. Eng. Chem. Prod. Res. Div.* **22**, 40 (1983).
21. Dhandapani, B., Ramanathan, S., Yu, C. C., Fruhberger, B., Chen, J. G., and Oyama, S. T., *J. Catal*. **176**, 61 (1998).
22. Tisher, R. E., Narain, N. K., Stiegel, G. J., and Cillo, D. L., *Ind. Eng. Chem. Prod. Res. Div*. **26**, 422 (1987).
23. Mickelson, G. A., U.S. Patent 3,755,150 (1968).
24. López Agudo, A., López Cordero, R., Palacios, J. M., and Fierro, J. L., *Bull. Soc. Chim. Belg*. **104**(4–5), 237 (1995).
25. Fierro, J. L. G., López Agudo, A., Esquivel, N., and López Cordero, R., *Appl. Catal*. **48**, 353 (1989).
26. López Cordero, R., Esquivel, N., Lázaro, J., Fierro, J. L. G., and López Agudo, A., *Appl. Catal*. **48**, 341 (1989).
27. Housm, E. C., and Lester, R., British Patent 807,583 (1959).
28. Poulet, O., Hubaut, R., Kasztelan, S., and Grimblot, J., *Bull. Soc. Chim. Belg. Eur. Sect.* **100**(11–12), (1991).
29. Colgan, J. D., and Chomitz, N., U.S. Patent 3,287,280 (1966).
30. Tolman, C. A., Druliner, J. P., Krusic, P. J., Nappa, M. J., Seidel, W.C., Williams, I. D., and Ittel, S. D., *J. Mol. Catal*. **48**, 129 (1988).
31. Goedken, V. L., and Ercolani, C., *J. Chem. Soc. Chem. Commun*. 378 (1984).
32. Gishti, K., Iannibello, A., Marengo, S., Morelli, G., and Titorelli, P., *Appl. Catal*. **12**, 381 (1984).
33. Craje, M. W. J., de Beer, V. H. J., and van der Krann, A. M., *Catal. Today* **10**, 337 (1991).
34. Cerda, J. L. R., and Prins, R., *Bull. Soc. Chim. Belg.* **100**, 815 (1991).
35. Mangnus, P. J., van Langeveld, A. D., de Beer, V. H. J., and Moulijn, J. A., *Appl. Catal*. **68**, 161 (1991).
36. Ramanathan, S., and Oyama, S. T., *J. Phys. Chem*. **99**, 16365 (1995).
37. Rundqvist, S., *Acta Chem. Scand.* **16**, 992 (1962).
38. Cullity, B. D., "Elements of X-Ray Diffraction," 2nd ed., Addison–Wesley, Menlo Park, CA, 1978.
39. Li, X., Wang, W., Li, H., and Deng, J.-F., *J. Catal.* **194**, 211 (2000).
40. Hodnett, B. K., and Delmon, B., *Stud. Surf. Sci. Catal.* **27**, 53 (1986).
41. van Parijs, I. A., Froment, G. F., and Delmon, B., *Bull. Soc. Chim. Belg.* **93**, 823 (1984).
42. Marzari, J. A., Rajagopal, S., and Miranda, R., *J. Catal.* **156**, 255 (1995).
43. Jian, M., and Prins, R., *J. Catal.* **179**, 18 (1998).
44. Rota, F., and Prins, R., *J. Mol. Catal. A* **162**, 359 (2000).
45. Rota, F., Ranade, V. S., and Prins, R., *J. Catal.* **200**, 389 (2001).
46. Oyama, S. T., *in* "Preparation of Solid Catalysts" (G. Ertl, H. Knözinger, and J. Weitkamp, Eds.), p. 139. Wiley–VCH, Weinheim, 1999.
47. Pecoraro, T. A., and Chianelli, R. R., *J. Catal*. **67**, 430 (1981).
48. Oyama, S. T., Wang, X., Requejo, F., Sato, T., and Yoshimura, Y., *J. Catal.* **209**, 1 (2002).